



An effective strategy to improve dynamic and cyclic stability of HQC/TiO₂ photocatalyst by introducing carbon quantum dots or iron ion via metal-complex

Dandan Ni^a, Qingkun Shang^{a,*}, Tongtong Guo^a, Xinyue Wang^a, Yongmei Wu^{b,*}, Hongyu Guan^{a,*}, Dan Wang^a, Min Zhang^a

^a Northeast Normal University, Changchun, 130024, Jilin, PR China

^b Department of Chemical and Environmental Engineering, Xinjiang Institute of Engineering, Urumqi, 830091, Xinjiang, PR China

ARTICLE INFO

Article history:

Received 31 December 2016

Received in revised form 23 March 2017

Accepted 6 April 2017

Available online 9 April 2017

Keywords:

Dynamic and cyclic stability

Carbon quantum dots

Interfacial interaction and electron transport

Photocatalysis under visible light

ABSTRACT

A novel photocatalyst, 8-hydroxy-Quinoline-7-carboxylic acid/TiO₂ (HQC/TiO₂) was synthesized and used to decompose phenol under visible light irradiation. It exhibited excellent photocatalytic activities, about 95.9% of phenol can be degraded after 2 h visible light illumination. However, the recycling efficiency is not very ideal. In order to improve its photostability during recycling process, we had adopted a novel and effective strategy for the introduction of carbon quantum dots or iron ions into the photocatalytic system. Two other novel catalysts, CQDs/HQC/TiO₂ and Fe(HQC)₃/TiO₂ were prepared. After investigated the structure and morphology characteristics of HQC/TiO₂, CQDs/HQC/TiO₂ and Fe(HQC)₃/TiO₂ by analysis of X-ray diffraction, FTIR spectra, UV-vis absorption and diffuse reflectance spectra, X-ray photoelectron spectroscopy, transmission electron microscopic and photoelectrochemical properties, the possible and different photocatalytic mechanisms for these three photocatalysts were proposed. On the basis of this, the key factors affecting the dynamic and cyclic stability of HQC/TiO₂ by introducing CQDs or Fe³⁺ ions via Fe-HQC complex were explored.

© 2017 Elsevier B.V. All rights reserved.

1. Introduction

It is generally known that an ideal photocatalyst should have both a wide range of photoabsorption and a high separation efficiency of the photo-induced charge carriers [1]. As a star photocatalyst, titanium dioxide has been widely used for photocatalytic degradation of organic pollutants in water and air under UV irradiation due to its excellent performance, such as high catalytic activity, light stability, low cost, safe and non-toxic [2–8]. Unfortunately, it is still a challenge to improve its lower usage of sunlight and higher recombination rate of photo-generated charge carriers, which become two of the huge obstacles in practical application. In many strategies to improve the photocatalytic activity of TiO₂, the dye sensitization has attracted much attention in recent years [9–11]. On the one hand, the dye often has a large conjugated structure, with a strong visible light capture capability. On the other hand, the highest occupied molecular orbital (HOMO) and lowest

unoccupied molecular orbital (LUMO) levels of most dye molecules are well matched with the band structure of TiO₂, which promotes the effective separation of the electron and the hole. But there are still some problems to be solved in the application of photocatalytic degradation of organic pollutants. For example, when the dye molecules absorb the visible light, the electrons can transfer from the HOMO to the LUMO, these excited electrons are easily moved to the conduction band (CB) of titanium dioxide, so that the visible light photocatalytic activity of titanium dioxide appeared. In this process dye is oxidized due to lost electrons. In general, less dye molecules combined to the surface of titanium dioxide. If the dye molecules cannot obtain electrons from the environment to supplement the missing electrons, the self-degradation of dye will happen, which is the main reason leads to the decrease of photocatalytic efficiency and photostability of the composite photocatalyst in recycling. So, the key to avoid the self-degradation of dye is to prevent the oxidation reduction reaction occurring on the dye. Introducing electron donors is a good strategy.

Carbon quantum dots (CQDs) have become a promising candidate for photocatalysis application due to its unique optical adsorption characteristics, photo-induced electron transfer, photoluminescence, and electron reservoir properties. They have

* Corresponding authors.

E-mail addresses: shangqk995@nenu.edu.cn (Q. Shang), wuyongmeismx@163.com (Y. Wu), guanh@nenu.edu.cn (H. Guan).

been applied in combining with hematite [12], BiOX(X=Br,Cl) [13,14], Bi₂WO₆ [15,16], BiVO₄ [17], C₃N₄ [18], Ag₃PO₄ [19] and TiO₂ [20]. Kang's group reported a highly efficient photoelectric conversion system by introducing CQDs as an electron transfer intermediary [21–24]. The CQDs they obtained according to electrochemical method have a structure similar to that of the polycyclic aromatic hydrocarbons, and the surface contains abundant functional groups. This unique structure makes the CQDs not only have very good fluorescence properties, but also have excellent electron transport properties. Zhang et al. report the facile one-step fabrication of Fe₂O₃/CQDs composites, which show improved photocatalytic performance for the degradation of toxic gas under visible light. They proposed a reasonable model to illustrate the key roles of CQDs in the photocatalytic process [25]. Pradipta Purkayastha's group reported the ultra-fast photoinduced electron transfer between carbon nanoparticles and cyclometalated rhodium and iridium complexes [26]. They proposed that light-harvesting features of four cyclometalated complexes of Ir(III) and Rh(III) contributed toward photogenerated electron and energy transfer for solar energy conversion and photocatalysis. The electron injection from the complexes to the carbon nanoparticles (CNPs) had been confirmed via the quenching of CNPs fluorescence and electrochemical measurements. H. Zhang et al. prepared carbon dots by electrochemical method and constructed CDs/Ag/Ag₃SO₄ composite catalyst. They found that CDs/Ag/Ag₃SO₄ is more stable in the degradation reactions of methylene blue under visible light radiation. During the repeating the photocatalytic processes, the catalytic efficiency has almost no change [27].

In a word, there were many reports in the literature about the interaction between CQDs and semiconductor or complex, directly. Inspired by their works we synthesized CQDs from chitosan and used it to improve the dynamic and cyclic stability of HQC/TiO₂. Comparing to our previous work [28] we also investigated the dynamic and cyclic stability of Fe(HQC)₃/TiO₂. The experimental results showed that the dynamic and cyclic stability of the composite photocatalyst could be improved effectively by using both of CQDs and Fe³⁺ ions. In particular, the introduction of CQDs, not only makes the photocatalyst to maintain a very high recycling efficiency, but also speeds up the rate of photocatalytic reaction. Introducing CQDs with different structures and characteristics into the study of photocatalysis is of great significance to further expand the application field of CQDs and to elucidate its mechanism. The comparison of the effects of CQDs and metal ions via complexes on the photocatalytic system has not been reported.

2. Experimental

2.1. Synthesis

Preparation of TiO₂ nanoparticles: Experiments were carried out by using the traditional hydrothermal method. After adding 15.0 ml of anhydrous ethanol, 6.0 ml of tetrabutyl titanate (TBOT) was added, dropwise, to a 50 ml beaker, the yellow transparent solution was obtained. Then 9.0 ml of deionized water was added into the above solution. Keep stirring for 0.5 h under room temperature. The suspension was then transferred to 50 ml poly-tetrafluoroethylene (PTFE) equipped autoclave continued to react for 2 h at 120 °C. After cooling to room temperature naturally the precipitation was centrifugal separation and washed with distilled water and ethanol for three times, respectively, then drying in vacuum oven at 80 °C. The precursor was calcined at 500 °C for 4 h to form TiO₂ nanoparticle.

Preparation of Fe(HQC)₃ complex: 0.028 g of 8-hydroxy-Quinoline-7-carboxylic acid (HQC) was dissolved in 30 ml deionized water. Then 0.020 g iron nitrate (Fe(NO₃)₃·9H₂O) was added to the solution under vigorous stirring. The color of solution changes from light yellow to reddish brown immediately. Keep stirring 1 h continuously. The solid complex was obtained by drying the solution at 80 °C. There are two possible structures for Fe(HQC)₃ when two different coordination models were adopted (see Fig. 1).

Preparation of CQDs: the CQDs were synthesized using the hydrothermal method. As carbon source 0.2 g of chitosan was dissolved in 30 ml 1% acetic acid solution. After stirring for 1 h, the gel was formed and sealed in a 50 ml Teflon-lined autoclave for 24 h at 160 °C. The autoclave was allowed to cool down naturally, and the obtained brown solution was filtrated to remove the unreacted moieties.

Preparation of HQC/TiO₂ and Fe(HQC)₃/TiO₂ photocatalysts: A certain amount of titanium dioxide particles were dispersed to 30 ml HQC or Fe(HQC)₃ solution, stirring for an hour, and then transferred to the lining of reactants for PTFE high-pressure reaction kettle. The hydrothermal treatment system was carried out at 140 °C, and maintained for 7 h. After that the obtained suspension was cooled to room temperature, centrifuged, washed with water and ethanol and then dried at 80 °C.

Preparation of CQDs/HQC/TiO₂ photocatalysts: A certain amount of HQC/TiO₂ particle was added to CQDs solution. Keep stirring for 1 h, and then transferred to the lining of reactants for PTFE high-pressure reaction kettle. The hydrothermal treatment system was carried out at 140 °C, and maintained for 7 h. After that the obtained suspension was cooled to room temperature, centrifuged, washed with water and ethanol and then dried at 80 °C.

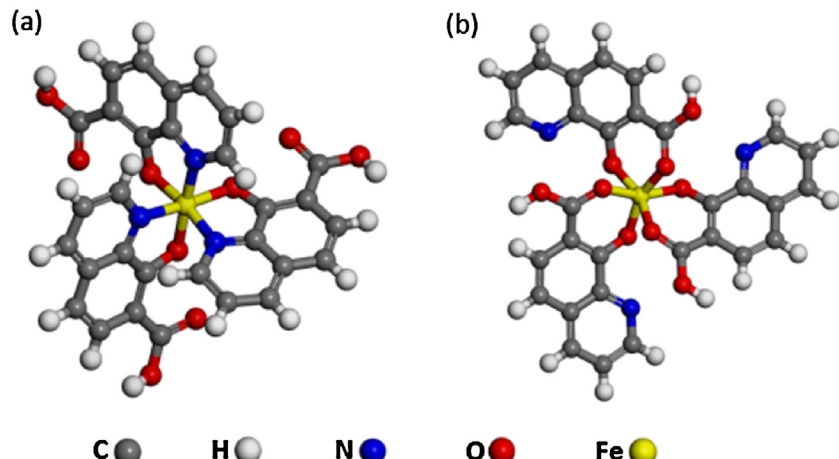


Fig. 1. Two possible structures of Fe(HQC)₃ complex derived from two different coordination models.

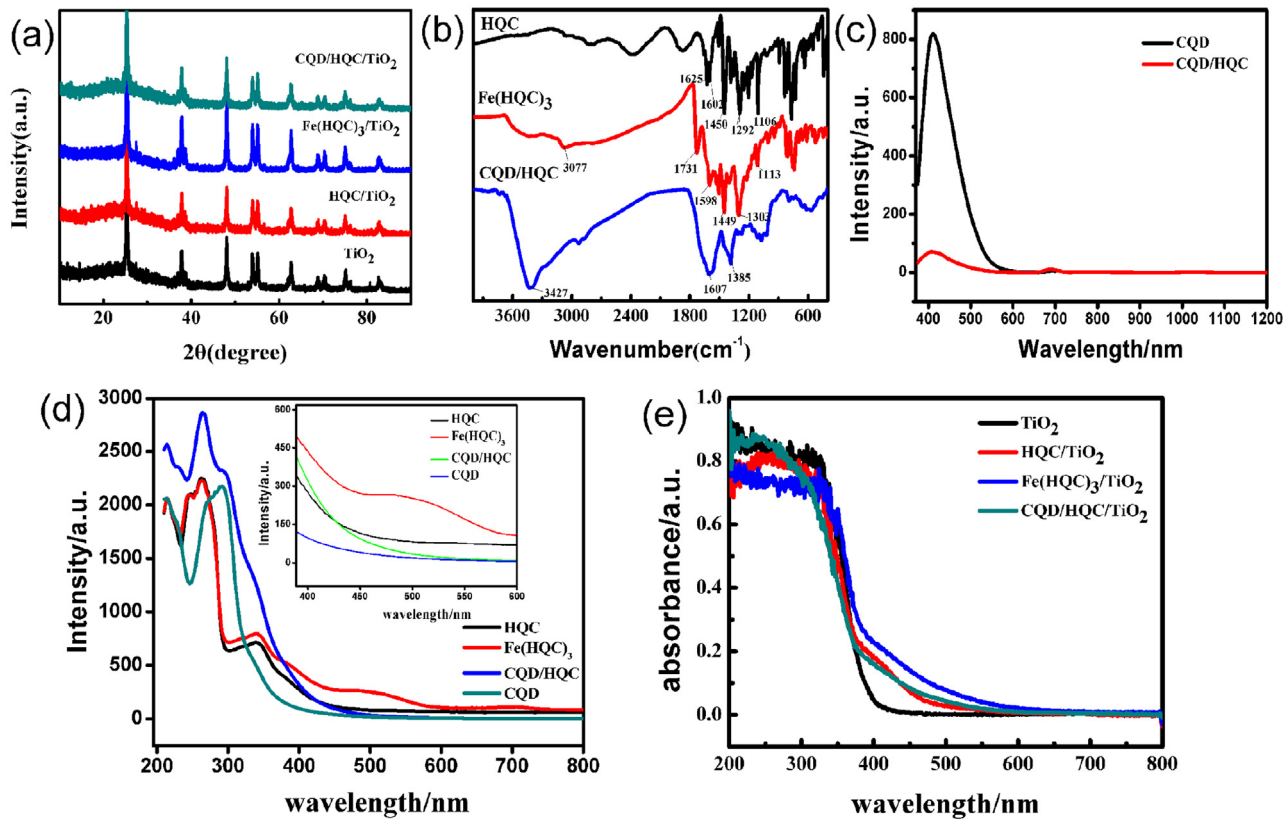


Fig. 2. (a) XRD patterns of four different catalysts. (b) IR spectra of HQC, $\text{Fe}(\text{HQC})_3$ and CQDs/HQC. (c) Fluorescence spectra of CQDs and CQD/HQC. (d) UV-vis adsorption spectra of HQC, $\text{Fe}(\text{HQC})_3$, CQD and CQD/HQC. (d) UV-vis DRS of four different catalysts.

2.2. Characterizations

The crystal structures of the prepared photocatalysts were examined by X-ray diffraction (XRD) using a Kigaku.D/Max-rA with Cu K radiation and transmission electron microscopic (TEM, JEOL 100 CXII). The FTIR spectrum was analyzed with Fourier transform infrared spectrometer (FTIR, Nicolet Magna 560). UV-vis diffuse reflectance spectra (DRS) were obtained by using an UV-vis-NIR spectro-photometer (CARY500Scan). Ground-state redox potentials of Fe-complexes were determined with a standard three-electrode configuration CHI830b with a modified glassy carbon electrode serving as the working electrode, and Ag/AgCl (in saturated KCl solution) and platinum wire serving as reference electrodes and the counter, respectively. X-ray photoelectron spectroscopy (XPS) data were obtained using a Thermo Scientific ESCALAB 250Xi photoelectron spectrometer.

2.3. Photocatalytic evaluation

The photocatalytic activity of the catalyst was evaluated by the photodegradation of phenol. 50 mg catalyst was dispersed in a beaker which containing 50 ml 10 mg/L phenol solution. A 300 w xenon lamp with a cut-off filter (<400 nm) was used for illumination, and the reaction device equipped with magnetic stirring and condensing system, to ensure the stability of the reaction condition. The dispersion was stirred for 30 min in the dark, so as to facilitate the adsorption balance of the catalyst surface, then illumination experiment (2 h), at a certain time interval, 5 ml of the reaction solution was taken out and centrifuged at 8000 rpm to remove the catalyst. The concentration of phenol was tested by using Agilent 1200 high performance liquid chromatograph.

3. Results and discussion

3.1. Crystal structure and composition of the composite catalyst

The phase structure of photocatalysts were measured by X-ray diffractometer and shown in Fig. 2(a). Comparing to standard pattern of anatase (JCPDS 21–1272), pure TiO_2 and all three composite catalyst, HQC/TiO_2 , $\text{Fe}(\text{HQC})_3/\text{TiO}_2$ and CQDs/HQC/TiO₂, had a single phase anatase, which indicates that hydrothermal process did not change the phase of TiO_2 . The particle size calculated according to Scherrer Equation and crystal parameter of TiO_2 and other three composite catalysts were exhibited in Table 1. Compared to 25.35 nm of pure titanium dioxide the average particle size of other three composite catalysts, HQC/TiO_2 , $\text{Fe}(\text{HQC})_3/\text{TiO}_2$ and CQDs/HQC/TiO₂, increased to 27.89 nm, 28.31 nm and 28.22 nm, respectively. Slight changes of crystal parameter can be found after HQC, $\text{Fe}(\text{HQC})_3$ and CQDs/HQC were combined with TiO_2 which indicated tiny lattice distortion appeared.

The infrared spectra (IR) of HQC, $\text{Fe}(\text{HQC})_3$ and CQDs/HQC were characterized and illustrated in Fig. 2(b). For the pure organic matter HQC, five characteristic absorption peaks belong to $\text{C}=\text{O}$ (1625 cm^{-1}), $\text{C}=\text{N}$ (1602 cm^{-1}), $\text{C}=\text{C}$ (1450 cm^{-1}), $\text{C}=\text{O}$ vibra-

Table 1
Particle size and crystal parameter of four catalysts.

Photocatalytics	Crystal phase	Crystal size(nm)	Crystal parameter(nm) [29]		
			a	b	c
TiO_2	A	25.39	3.7803	3.7803	9.4867
HQC/TiO_2	A	27.98	3.7784	3.7784	9.5091
$\text{Fe}(\text{HQC})_3/\text{TiO}_2$	A	28.31	3.7836	3.7836	9.4921
CQD/HQC/TiO ₂	A	28.22	3.7823	3.7823	9.5077

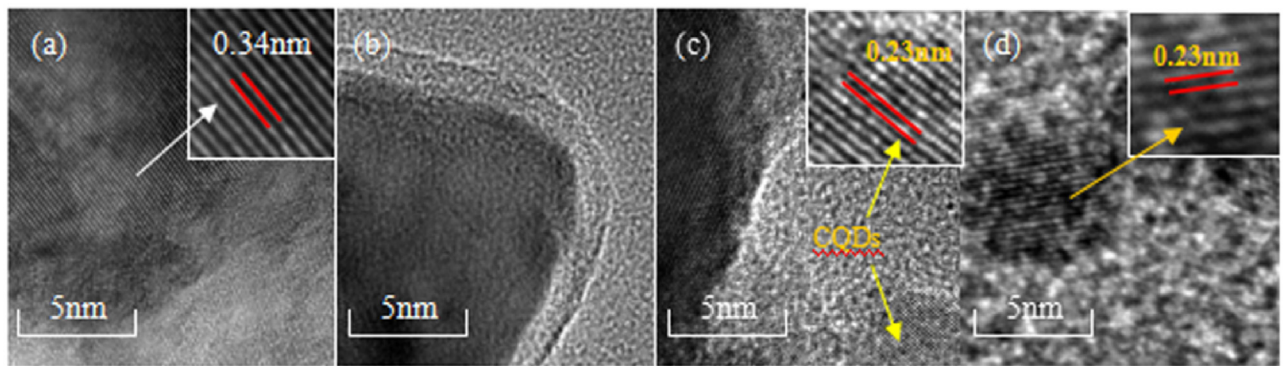


Fig. 3. HRTEM image of HQC/TiO₂ (a), Fe(HQC)₃/TiO₂ (b), CQDs/HQC/TiO₂ (c) and CQD (d).

tion (1292 cm⁻¹, 1106 cm⁻¹) respectively. After coordination with Fe(III), vibration absorption peak of C=N moved to 1598 cm⁻¹, C—O vibration increase to 1303 cm⁻¹ and 1113 cm⁻¹. And a wider hydroxyl absorption peak appeared which suggested that phenolic oxygen bonding with metal ions. This indicates that the iron is coordinated with the hydroxyl oxygen atom and nitrogen atom and formed the bidentate ternary chelate. Due to the effect of conjugate of the carbonyl and quinoline ring, the C=O vibration move to the high wavenumber, thus has obvious absorption peak in 1731 cm⁻¹, and this means the carboxyl oxygen does not participate in coordination. So the structure of Fe(HQC)₃ complex is possible presented in Fig. 1(a). For CQD/HQC, absorption peaks in 1385 cm⁻¹ and 3427 cm⁻¹ are derived from the hydroxyl groups on the surface of CQD. At the same time, because of its surface rich carboxyl, C=O and C=N vibration absorption peaks coincided together.

From Fig. 2c we can find that the fluorescence properties of CDQs were greatly changed after the interaction with HQC. The fluorescence intensity of CQDS emission at about 430 nm decreased from 800 to less than 100a.u, which indicated the combination of HQC and CQDS leads to the quenching of CQDs fluorescence. This may be the migration of electrons from the HQC to the CQDs. Collisions between electrons lead to the release of energy in the form of non-fluorescent radiation.

The UV-vis adsorption spectra of HQC, Fe(HQC)₃, CQDs and CQDs/HQC are illustrated in Fig. 2(d). Comparing to the absorption of HQC, an obvious enhanced absorption, belonging to Fe(HQC)₃, appeared in visible region centered at about 500 nm (see insert of Fig. 2d). It is due to the introduction of metal ions, M-L transition between metal and ligands. There is a small absorption peak at about 700 nm, should be the characteristic absorption of the iron ion. After combining with HQC, the maximum absorption peak of CQDs appeared at 300 nm becomes to a shoulder peak. At the same time the absorption peak of HQC at 345 nm also becomes less obvious. But the band edge absorption of HQC—CQDs extended to visible light clearly.

From the UV-vis diffuse reflection absorption (DRS) of TiO₂, HQC/TiO₂, Fe(HQC)₃/TiO₂, CQDs/HQC/TiO₂ shown in Fig. 2(e) we can calculated their band gap are 3.2 eV, 2.79 eV 2.47 eV and 2.60 eV by using Tauc plots, respectively. Under the same condition, the enlarged scope of visible light absorption appeared except TiO₂, it indicated that the enhanced visible light absorption property (from 400 to 600 nm) can be realized when HQC, Fe(HQC)₃ and CQDs/HQC were used to react with TiO₂.

In order to further prove the composition of catalysts, the high resolution transmission electron microscopy (HRTEM) was carried out. The image of HQC/TiO₂, Fe(HQC)₃/TiO₂, CQDs/HQC/TiO₂ and CQDs are shown in Fig. 3. From Fig. 3a and b, it is clearly that a layer of amorphous materials had been attached to the surface of TiO₂,

which demonstrated the successful combination between HQC or Fe(HQC)₃ with TiO₂ photocatalysts. From Fig. 3c, we can find the particle about 4 nm which have a lattice distance of 0.23 nm. It corresponds to that of CQDs shown in Fig. 3d exactly. So, it can be proved that CQDs had scattered over the surface of HQC/TiO₂.

XPS results in Fig. 4 provide further evidence that sensitizers indeed formed composites with TiO₂. Peaks at 458.2 eV and 464.0 eV in Fig. 4a, 458.6 eV and 464.4 eV in Fig. 4b, 458.3 eV and 464.0 eV in Fig. 4c, are assigned to Ti 2p_{3/2} and Ti 2p_{1/2}. All the distance between these two peaks are 5.8 eV, which indicates the crystal structure of TiO₂ unchanged after forming composite catalysts. Peaks of Fe 2p_{1/2} and Fe 2p_{3/2} are detected at 724.8 eV and 710.9 eV, which belongs to Fe³⁺ ion [30]. The appearance of peaks N 1s illustrate the surface of TiO₂ has been contaminated by organic compounds. One interesting thing is the bonding energy of O1s appears relatively large changes in three composites. Compared to Ti-O peak located at 529.3 eV for HQC/TiO₂ in Fig. 4a, the peak intensity of 529.7 eV (in Fig. 4b) for Fe(HQC)₃ complex decreased. Two peaks belonging to C—O—C and C=O at 531.4 eV and 532.8 eV in Fig. 4a are nearly the same as that in Fig. 4b, but merge into one peak in Fig. 4c. These bond energy changes related to oxygen, just explain the difference surface interaction between HQC, Fe-HQC complex, CQDs and TiO₂ [31].

3.2. Photocatalytic performance and photostability

To evaluate and compare the photocatalytic performance of HQC/TiO₂, Fe(HQC)₃/TiO₂ and CQDs/HQC/TiO₂, a series of contrast experiments were performed and the degradation results under different conditions were shown in Fig. 5a. First, phenol solution was put at certain time illumination conditions, while excluding catalyst testing its degradation rate, and almost no degradation of phenol. Second, the phenol system containing catalyst was placed in dark state, and the degradation effect of phenol was detected. Due to the adsorption on the surface of the catalyst, phenol concentration slightly decreased, negligible. And finally, the changes of the concentration of phenol were detected after the reaction of phenol with TiO₂, CQDs/TiO₂, HQC/TiO₂, Fe(HQC)₃/TiO₂ and CQDs/HQC/TiO₂ five different catalysts under visible light illumination. In the case of pure TiO₂ only 35.4% of phenol was degraded. About 70% of phenol was decomposed when CQDs/TiO₂ was served as photocatalyst. However, it was found that about 96% of phenol was degraded when HQC/TiO₂, Fe(HQC)₃/TiO₂ and CQDs/HQC/TiO₂ were used as catalysts, respectively. Obviously, after combining with HQC, Fe(HQC)₃ and CQDs/HQC the photocatalytic activity of TiO₂ increases greatly. The degradation rate of phenol in 2 h was almost the same indicated the effects of them on the photocatalytic property of TiO₂ was the same.

The speed of the photocatalytic reaction is another important indicator for the evaluation of the photocatalyst. The kinetics process of degradation reaction of phenol by TiO_2 , HQC/TiO_2 , $\text{Fe}(\text{HQC})_3/\text{TiO}_2$ and $\text{CQDs}/\text{HQC}/\text{TiO}_2$ is shown in Fig. 5b. In 80 min, the kinetic constants (k) were 0.0024 min^{-1} , 0.0268 min^{-1} , 0.0234 min^{-1} and 0.0333 min^{-1} corresponding to TiO_2 , HQC/TiO_2 , $\text{Fe}(\text{HQC})_3/\text{TiO}_2$ and $\text{CQDs}/\text{HQC}/\text{TiO}_2$. It is pointed out that the kinetic constants (k) increased about 10 times as the composite catalyst compared to pure titanium dioxide. It also indicated when $\text{CQDs}/\text{HQC}/\text{TiO}_2$ was the photocatalyst, the degradation speed of phenol was the fastest.

The photostability of the catalyst is an important aspect to judge whether it has practical value, so the recycled photocatalytic experiments were carried out and the results were presented in Fig. 5c. Clearly, CQDs/HQC/TiO₂ catalyst showed the best photostability in the three catalysts, 97.1%, 96.6% and 95.5% of phenol were decomposed after the first, second and third usage of CQD/HQC/TiO₂. When Fe(HQC)₃/TiO₂ was used as catalyst, the degradation efficiency of phenol declined from 96.4% to 83.3% and 55.7%. However, the decrease is more noticeable for HQC/TiO₂, only 72.5%, and 48.3% of phenol can be decomposed in the second and third recycling use, comparing to 95.9% of the first time employed. This shows that the

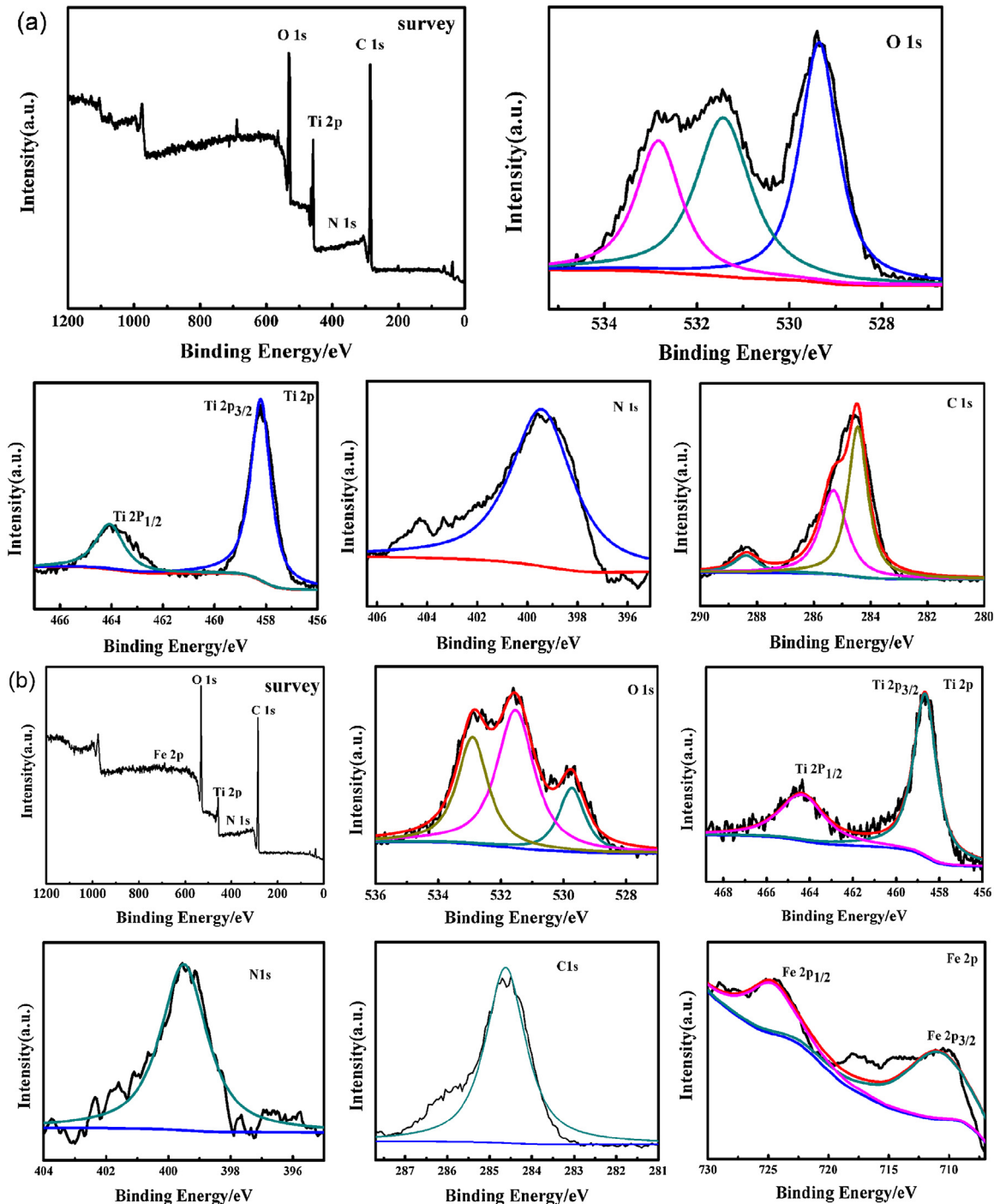


Fig. 4. (a) XPS spectra of HQC/TiO₂ (b) XPS spectra of Fe(HQC)₃/TiO₂ (c) XPS spectra of CQDs/HQC/TiO₂.

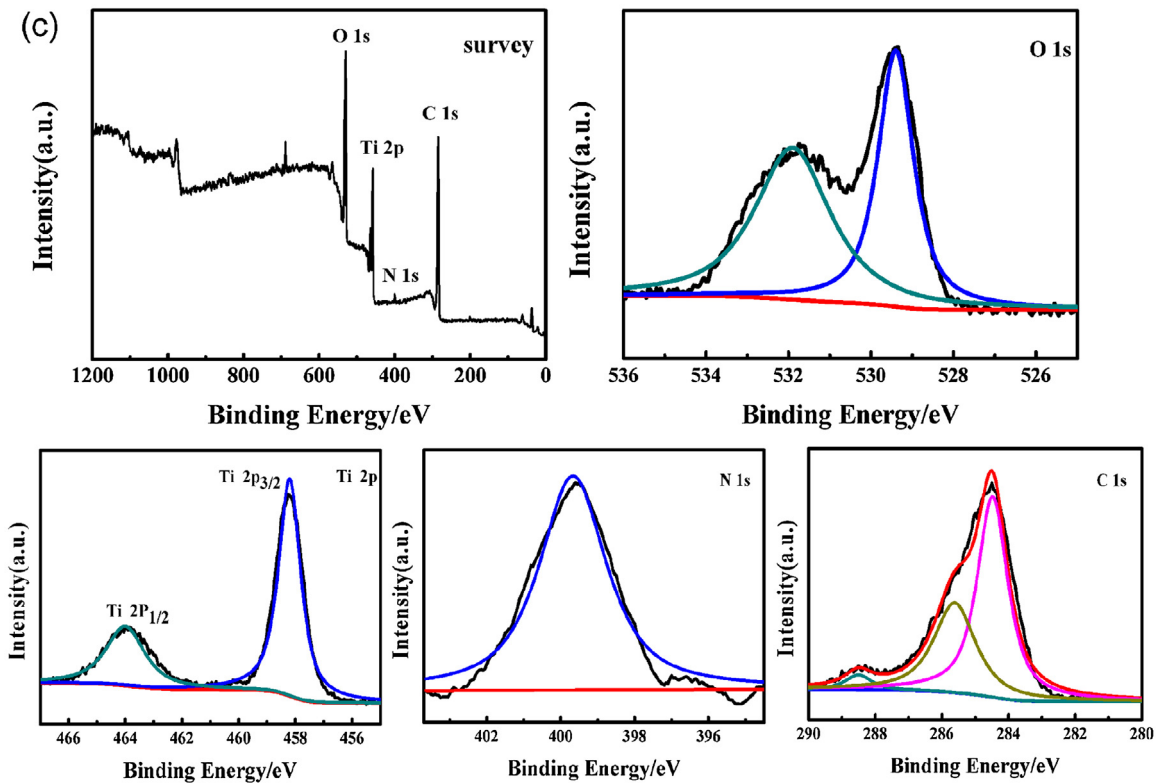


Fig. 4. (Continued)

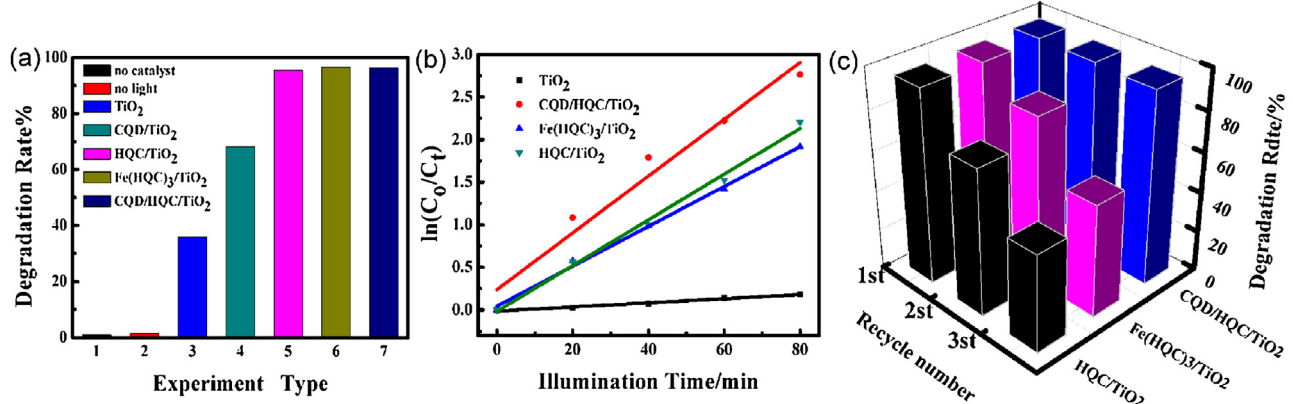


Fig. 5. (a) Degradation efficiency of phenol under different condition. (b) Kinetic fitting curves of the photocatalytic degradation of phenol. (c) Recycling effect of composite catalysts.

photostability of HQC/TiO₂ can be improved via forming Fe-HQC complex or combining with CQDs.

3.3. Mechanism

Why HQC can improve the photocatalytic performance of TiO₂ under visible light, but the photostability is not good enough? From Fig. 2d we can find the band edge absorption of HQC can be extended to 450 nm, and the band gap is 2.79 eV calculated according to Tauc plots. The HOMO and LUMO energy level are –5.23 eV and –2.44 eV via electrochemical test, which matching with the CB and VB energy level of TiO₂ very well. So, the electron transition from HOMO to LUMO achieved under visible light irradiation. Then, these excited electrons moved to the CB of TiO₂ and captured by O₂ on the surface of TiO₂. Superoxide radicals formed for degradation of phenol. Because of the special molecular structure of HQC,

there are three possible chelating modes (shown in Fig. 6a) when it combined with TiO₂ by using –COOH alone, –COOH and –OH, or –OH and –N together. There are two main reasons for the decline of the optical stability. One is the competition of three different chelating modes with each other and the formation of hydrogen bonds between the HQC molecules which weakens its chelating effect with TiO₂, resulting in the loss of HQC molecules from the TiO₂ surface. The other is the self-degradation due to losing excited electrons [31].

The effect of Fe-HQC complex on visible light photocatalytic performance of titanium dioxide is different from that of HQC. There is an obvious visible absorption region centered at about 500 nm on UV-vis absorption spectrum of Fe(HQC)₃ (see Fig. 2d), which is the result of M-L transmission. The band gap 2.47 eV calculated according to Tauc plots is corresponding to the HOMO and LUMO energy

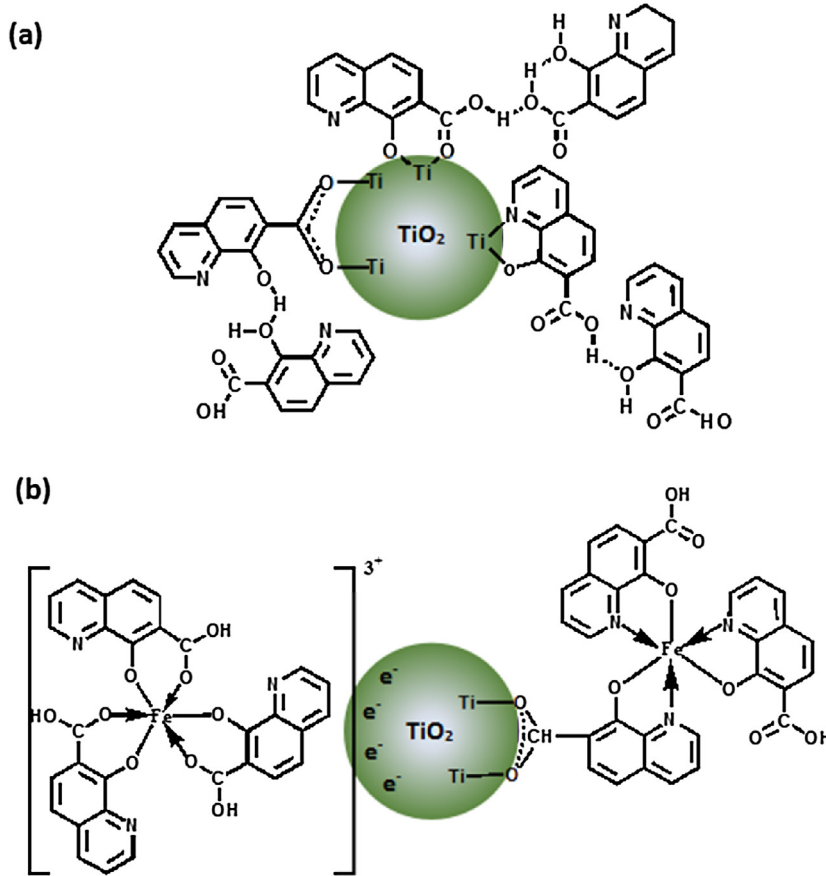


Fig. 6. Schematic presentations of binding of HQC(a) and Fe(HQC)₃(b) on the TiO₂ surface.

level -5.27 eV and -2.80 eV, which matching with the CB and VB energy level of TiO₂ very well. So, the electron transition from metal to HQC appeared under visible light irradiation. Then, these excited electrons moved to the CB of TiO₂ and captured by O₂ on the surface of TiO₂ to form superoxide radicals that is the main group for degradation of phenol. The electrons used for the photocatalytic are derived from the transition metal ions, rather than the HQC, so there is no self-degradation of HQC. But the light stability is still not ideal, what is the reason? It may be related to the interaction of HQC with the TiO₂ surface. From Figs. 1 and 6b we can find there are two possible structures of Fe(HQC)₃ complex derived from two different coordination models. To the structure a (Fig. 1a), the residual carboxyl group of HQC interacts with the Ti on the TiO₂ surface. To the structure b (Fig. 1b), the combination between Fe(HQC)₃ and TiO₂ depends on the electrostatic interactions, which is much weaker than that of the former. It is very easy to fall off from the surface of TiO₂ during the recycle process, thus results in the decline of the photocatalytic activity of Fe(HQC)₃/TiO₂.

It is shown in Fig. 2d that CQDs has obvious visible light absorption properties. In this way, we can understand why CQDs/TiO₂ under the same conditions can make 70% of phenol degradation (see Fig. 5a). From the absorption spectrum of CQDs/HQC shown in Fig. 2d, the interaction between the CQDs surface groups and HQC leads to the enhanced visible light absorption property of HQC. But this does not explain why the CQDs/HQC/TiO₂ exhibited the fastest phenol degradation efficiency and the best photo-stability in recycling. The excellent electron donor-receptor properties and electronic conductivity of CQDs are possible the keys to these two problems. First, for titanium dioxide, the number of electrons in its CB is increased due to the simultaneous acceptance of excited electrons from CQDs and HQC. Second, electrons can migrate between

CQDs and HQC. On the one hand, those electrons transport from HQC to CQDs, which may obtain the energy from the fluorescence quenching of CQDs, are quickly transferred to the CB of TiO₂, with the help of the mesh structure of the CQDs. On the other hand, electrons can transport from CQDs to HQC, thus results the lost electrons of HQC is supplied to avoid the occurrence of the HQC self-degradation. So, among three composite catalysts, CQDs/HQC/TiO₂ not only has the fastest photocatalytic activity but also the best photostability of phenol.

In order to further understand the optoelectronic properties of three catalysts HQC/TiO₂, Fe(HQC)₃/TiO₂, CQD/HQC/TiO₂, their photocurrent density were tested and the results were shown in Fig. 7(a). It is quite clear that the photocurrent densities derived from HQC/TiO₂, Fe(HQC)₃/TiO₂ and CQD/HQC/TiO₂ are all much higher than that of TiO₂. They are 8.04 , 11.1 , 10.8 $\mu\text{A}/\text{cm}^2$ respectively, compared with the 3.02 $\mu\text{A}/\text{cm}^2$ of TiO₂. The higher the photocurrent density means the longer the lifetime of photogenerated charges, thus the better photoelectric activity. In addition, the photocurrent density both of Fe (HQC)₃/TiO₂ and CQDs/HQC/TiO₂ are also greater than that of HQC/TiO₂. It demonstrated that the coexistence of two kinds of chelating modes affected the whole plane of HQC on the surface of TiO₂ and further hindered the smooth movement of electrons. On the contrary, larger conjugate structure of complex or plane and network structure of CQDs are all beneficial for the transmission of the optical electron. Fig. 7b-d shown the photocurrent density of HQC/TiO₂, Fe(HQC)₃/TiO₂ and CQD/HQC/TiO₂ during the three cycles. It may help us to explain the different photostability of these three catalysts. For HQC/TiO₂, after second and third cycles, the photocurrent density decreased greatly. And for Fe(HQC)₃/TiO₂, the decrease of the photocurrent density is weakened. But for CQD/HQC/TiO₂, it is almost unchanged

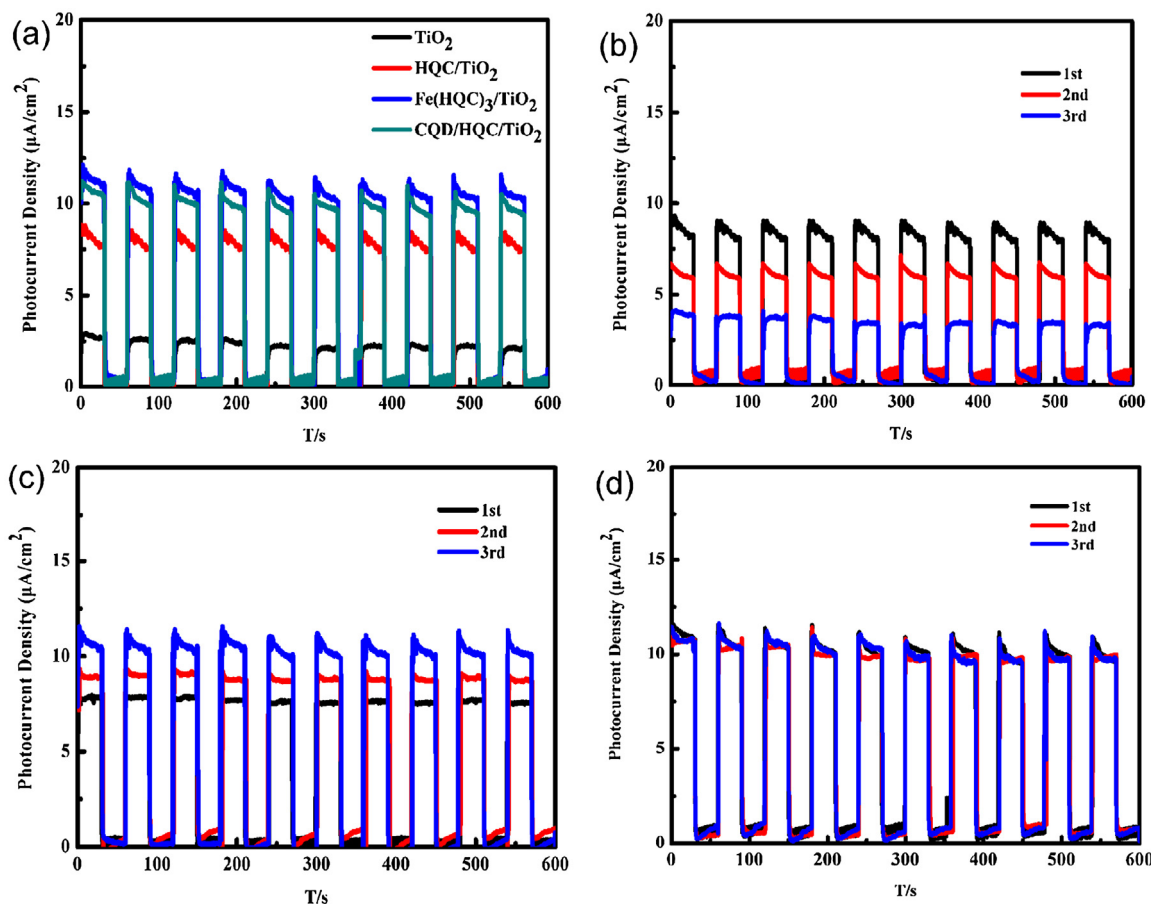


Fig. 7. (a) Photocurrent density of TiO_2 , HQC/TiO₂, Fe(HQC)₃/TiO₂ and CQD/HQC/TiO₂. Photocurrent density of HQC/TiO₂ (b), Fe(HQC)₃/TiO₂ (c), and CQD/HQC/TiO₂ (d) on recycling.

during the process of illumination, and the photocurrent density values keep in $10.8 \mu\text{A}/\text{cm}^2$. The change of the photocurrent density in the three cycles of these three catalysts is consistent with the experimental results of their photostability exhibited above. It can be concluded that the electron transport properties of the sensitizer are the key factors affecting the photostability of the TiO_2 composite photocatalyst [21,31].

4. Conclusions

The photocatalytic performance of TiO_2 under visible light was largely improved by HQC (8-hydroxy-Quinoline-7-carboxylic acid) as a sensitizer of TiO_2 , after irradiating 2 h, the photodegradation efficiency of phenol have been increased from 35.8% to 95.9% by using HQC/TiO₂ comparing to that of TiO_2 . But in the recycling process, its photocatalytic activity decrease a lot. To overcome this weakness, we used two effective strategies. One is to introduce Fe^{3+} to the surface of titanium dioxide in the form of $\text{Fe}(\text{HQC})_3$ complex. The other is to combine CQDs with HQC/TiO₂. The experimental results show that the high photocatalytic degradation efficiency of phenol was obtained, at the same time, the photostability was improved in different degree by using these two novel catalysts Fe(HQC)₃/TiO₂ and CQD/HQC/TiO₂. In particular, CQD/HQC/TiO₂ exhibited excellent dynamic and cyclic stability. The absorption properties, conjugated structure of $\text{Fe}(\text{HQC})_3$ complexes, and its binding mode with TiO_2 are the factors affecting the photocatalytic activity and stability of the catalyst. The Visible light absorption and fluorescence properties, electron donor and acceptor characteristics of CQDs and its excellent electron transport properties are the

key to accelerate the degradation rate of phenol and improve the photocatalytic activity and stability.

Acknowledgments

The authors would like to acknowledge the financial support by National Natural Science Foundation of China NSFC (21573039, 21667029, 51102042), Jilin Province Science and Technology Development Project (20140414021GH, 200905932), Jilin Province Environmental Protection Department Project (2008-22), and Jilin Province Personnel Department Project for supporting study abroad and return.

References

- [1] Z. Zhang, T. Zheng, X. Li, J. Xu, H. Zeng, Part Part Syst. Char. 33 (2016) 457–472.
- [2] F. Gao, X. Hou, A. Wang, G. Chu, W. Wu, J. Chen, H. Zou, Particuology 26 (2016) 73–78.
- [3] Z. Bian, F. Cao, J. Zhu, H. Li, Environ. Sci. Technol. 49 (2015) 2418–2424.
- [4] X.F. Qian, T. Kamegawa, K. Mori, H.X. Li, H. Yamashita, J. Phys. Chem. C 117 (2013) 19544–19551.
- [5] M.V. Dozzia, S. Marzoratia, M. Longhia, M. Codurib, L. Artigliac, E. Sellia, Appl. Catal. B: Environ. 186 (2016) 157–165.
- [6] J. Zhang, R. Li, X. Wan, Q. Li, J. Mater. Sci. Mater. Electron. 27 (2016) 2968–2973.
- [7] L. Li, Y. Feng, Y. Liu, B. Wei, J. Guo, W. Jiao, Z. Zhang, Q. Zhang, Appl. Surf. Sci. 363 (2016) 627–635.
- [8] S. Ivanov, A. Barylyak, K. Besaha, A. Bund, Y. Bobitski, R. Wojnarowska-Nowak, I. Yaremchuk, M. Kus-Liśkiewicz, Nanoscale Res. Lett. 11 (2016) 140–151.
- [9] X.-C. Li, G.-L. Jiang, G.-H. He, W.-J. Zheng, Y. Tan, W. Xiao, Chem. Eng. J. 236 (2014) 480–489.
- [10] F. Deng, L. Min, X. Luo, S. Wu, Nanoscale 5 (2013) 8703–8710.
- [11] Y. Park, S.-H. Lee, S.O. Kang, W. Choi, ChemComm 46 (2010) 2477–2479.
- [12] B.Y. Yu, S.-Y. Kwak, J. Mater. Chem. 22 (2012) 8345–8353.

- [13] J. Xia, J. Di, H. Li, H. Xu, H. Li, S. Guo, *Appl. Catal. B: Environ.* 181 (2016) 260–269.
- [14] F. Deng, X. Lu, F. Zhong, X. Pei, X. Luo, S. Luo, D.D. Dionysiou, C. Au, *Nanotechnology* 27 (2015) 065701–065712.
- [15] J. Di, J. Xia, Y. Ge, H. Li, H. Ji, H. Xu, Q. Zhang, H. Li, M. Li, *Appl. Catal. B: Environ.* 168–169 (2015) 51–61.
- [16] X. Qian, D. Yue, Z. Tian, M. Reng, Y. Zhu, M. Kan, T. Zhang, Y. Zhao, *Appl. Catal. B: Environ.* 193 (2016) 16–21.
- [17] F. Nan, Z. Kang, J. Wang, M. Shen, L. Fang, *Appl. Phys. Lett.* 106 (2015) 153901–153905.
- [18] S. Fang, Y. Xia, K. Lv, Q. Li, J. Sun, M. Li, *Appl. Catal. B: Environ.* 185 (2016) 225–232.
- [19] H. Zhang, H. Huang, H. Ming, H. Li, L. Zhang, Y. Liu, Z. Kang, *J. Mater. Chem.* 22 (2012) 10501–10506.
- [20] D. Yan, Y. Liu, C.-y. Liu, Z.-y. Zhang, S.-d. Nie, *RSC Adv.* 6 (2016) 14306–14313.
- [21] Z. Ma, Y.-L. Zhang, L. Wang, H. Ming, H. Li, X. Zhang, F. Wang, Y. Liu, Z. Kang, S.-T. Lee, *ACS Appl. Mater. Interface* 5 (2013) 5080–5084.
- [22] Z. Kang, Y. Liu, Chi Him A. Tsang, D.D.D. Ma, X. Fan, N.B. Wong, S.T. Lee, *Adv. Mater.* 21 (2009) 661–664.
- [23] Z. Kang, Chi Him A. Tsang, Z. Zhang, M. Zhang, N.-B. Wong, J. Antonio Zapien, Y. Shan, S.-T. Lee, *J. Am. Chem. Soc.* 129 (2007) 5326–5327.
- [24] Z. Kang, Chi Him A. Tsang, N.-B. Wong, Z. Zhang, S.-T. Lee, *J. Am. Chem. Soc.* 129 (2007) 12090–12091.
- [25] H. Zhang, H. Ming, S. Lian, H. Huang, H. Li, L. Zhang, Y. Liu, Z. Kang, S.-T. Lee, *Dalton Trans.* 40 (2011) 10822–10825.
- [26] S. Mondal, S.K. Seth, P. Gupta, P. Purkayastha, *J. Phys. Chem. C* 119 (2015) 25122–25128.
- [27] H.C. Zhang, H. Huang, H. Ming, H.T. Li, LL. Zhang, Y. Liu, Z.H. Kang, *J. Mater. Chem.* 22 (2012) 10501–10506.
- [28] Y. Huang, Q. Shang, D. Wang, S. Yang, H. Guan, Q. Lu, Shik Chi Tsang, *Appl. Catal. B: Environ.* 187 (2016) 59–66.
- [29] W. Wang, Q. Shang, W. Zheng, H. Yu, X. Feng, Z. Wang, Y. Zhang, G. Li, *J. Phys. Chem. C* 114 (2010) 13663–13669.
- [30] R. Miao, Z. Luo, W. Zhong, S.-Y. Chen, T. Jiang, B. Dutta, Y. Nasr, Y. Zhang, S.L. Suib, *Appl. Catal. B: Environ.* 189 (2016) 26–38.
- [31] H. Park, Y. Park, W. Kim, W. Choi, J. Photochem. Photobiol. C: Photochem. Rev. 15 (2013) 1–20.